Reduced Order Modeling Based on Multiport Cauer Ladder Network for Space Harmonics of Air-gap Flux Density in Cage Induction Motor

AUTHOR(S):

Takahashi, Yasuhito; Fujiwra, Koji; Sugahara, Kengo; Matsuo, Tetsuji

CITATION:

Takahashi, Yasuhito ...[et al]. Reduced Order Modeling Based on Multiport Cauer Ladder Network for Space Harmonics of Air-gap Flux Density in Cage Induction Motor. IEEE Transactions on Magnetics 2022, 58(8): 8203306.

ISSUE DATE:

2022-08

URL:

http://hdl.handle.net/2433/282116

Reduced Order Modeling Based on Multiport Cauer Ladder Network for Space Harmonics of Air-gap Flux Density in Cage Induction Motor

Yasuhito Takahashi[1], Koji Fujiwara[1], Kengo Sugahara[2], and Tetsuji Matsuo[3]

[1] Department of Electrical Engineering, Doshisha University, Kyotanabe 610-0394, Japan
[2] Faculty of Science and Engineering, Kindai University, Osaka 577-8502, Japan
[3] Graduate School of Engineering, Kyoto University, Kyoto 615-8510, Japan

This study investigated an efficient procedure for developing an accurate behavioral model of a cage induction motor (IM) based on the multiport Cauer ladder network (CLN). The CLN method was applied to a cage IM with semi-closed rotor slots as a model order reduction technique and a method for selecting the appropriate space harmonics included in the air-gap flux density, which is necessary for a multiport CLN method for induction machines, was discussed. Then, the developed approach was applied to the transient analysis of the cage IM coupled with a control system, and its effectiveness in terms of computational accuracy and cost was investigated.

***Index Terms*— Cage induction motor, Cauer ladder network, finite-element method, model order reduction, space harmonics.**

I. Introduction

To efficiently design a control system for electric machines, an accurate motor model, which enables circuit simulation with consideration to nonlinear magnetic properties and the change of a magnetic circuit caused by the rotation of the rotor under speed/torque control with acceptable computational cost, is required. Because the direct coupling of the finite-element method (FEM) with circuit simulation generally needs enormous computational costs, various model order reduction (MOR) techniques [1], [2] are frequently adopted to develop a current- and position-dependent motor model. The Cauer circuit has been reported as one of the MOR methods for eddy-current fields [3]-[5]. This approach is called the Cauer ladder network (CLN) method and has been extended to multiport problems [6] and nonlinear eddy-current fields [7].

Recently, the MOR approach based on the multiport CLN method for a cage induction motor (IM) has been proposed [6]. In this approach, first, the Cauer circuit representations for the stator and rotor domains are separately constructed. Then, the Cauer circuit corresponding to each domain is connected based on the boundary conditions for the space harmonics (SHs) of an air-gap flux density waveform. The MOR for cage IMs is inherently not straightforward even if linear magnetic properties are assumed in the rotor and stator because we should consider the electromotive force due to traveling waves at the airgap whose phase velocities in the rotor coordinate depend on the slip and on the space and time orders of SHs. This is why magnetostatic-based modeling is not effective to IMs and the choice of appropriate SHs is crucial to reconstruct torque waveforms including ripples. Although the multiport CLN approach in [6] accurately represents the numerical results obtained by the FEM with consideration to a sufficient number of SHs included in the air-gap flux density waveform, the excessive increase in the number of SHs leads to unacceptable computational cost. In addition, the treatment of nonlinear magnetic properties should be considered especially for cage IMs with closed rotor slots. Since skewed slots are usually adopted in general cage IMs, a modelling of it is also required. Among the issues to be solved in applying the multiport CLN method to practical cage IMs, the development of a method for selecting the dominant SHs is the most essential regardless of whether nonlinear magnetic properties and skewed rotor slots are considered or not because the number of SHs directly influences computational accuracy and efficiency.

With this background, this paper proposes a method for selecting the appropriate number of SHs included in the air-gap flux density waveform based on time and space harmonic analysis [8]. Furthermore, by considering the circuit connection of the rotor bars, a novel procedure was developed to derive the circuit parameters in the Cauer circuit, which satisfy the condition of the sum of the bar currents in the rotor domain always being zero [9]. Finally, the developed cage IM model was applied to a circuit simulation under speed control. The computational accuracy and cost of the FEM and multiport CLN method were compared to demonstrate the effectiveness of the proposed method in designing control system of cage IMs.

II. Method of Analysis

A. Multiport CLN Method for Cage Induction Motor

Fig. 1 shows a matrix CLN corresponding to the stator and rotor domain in a cage IM [6], in which the air-gap flux densities and phase currents/voltages are considered as the input data. A winding resistance R_s and the inductance matrices $\boldsymbol{L}_s$, $\boldsymbol{L}_h$, and $\boldsymbol{L}_{sh}$ are considered in the stator domain. Here, the 3-by-3 matrix $\boldsymbol{L}_s$ denotes the inductances of the primary windings, the M-by-M matrix $\boldsymbol{L}_h$ represents the inductance matrix corresponding to the SHs included in the air-gap flux density, the 3-by-M matrix $\boldsymbol{L}_{sh}$ represents the interactions between the

Manuscript received October 31, 2021; revised May 15, 2015 and June 1, 2015; accepted July 1, 2015. Date of publication July 10, 2015; date of current version July 31, 2015. Corresponding author: Y. Takahashi (e-mail: ytakahashi@mail.doshisha.ac.jp).

Color versions of one or more of the figures in this paper are available online at http://ieeexplore.ieee.org.

Digital Object Identifier (inserted by IEEE).

primary windings and the SHs, and M is the number of SHs. The multiport CLN method with several stages is applied to the rotor domain to consider the frequency characteristics of the eddy-current fields caused by the rotor bar currents. The number of stages is denoted as N. Because linear magnetic properties are assumed as a first step toward the practical use of the multiport CLN method, the cage IMs with semi-closed rotor slots are investigated. For reference, nonlinear MOR for cage IMs using the multiport CLN method is discussed in [10].

The number of rotor bars is not frequently divisible by the number of poles in a practical cage IM. In this case, when deriving appropriate circuit parameters in the Cauer ladder circuit, it is necessary to satisfy the condition of the sum of the rotor bar currents per pole-pair always being zero. To achieve this condition strictly by considering the circuit connection of the rotor bars, a novel procedure using the CLN method based on the $\boldsymbol{A}$-ϕ formulation [9] is proposed, where $\boldsymbol{A}$ is the magnetic vector potential and ϕ is the electric scalar potential. The resistance matrix $\boldsymbol{R}_{2n}$ and inductance matrix $\boldsymbol{L}_{2n+1}$ in the matrix Cauer circuit for the rotor domain can be determined as follows:

$$\boldsymbol{C}^{\mathrm{T}}\boldsymbol{M}_{\nu}\boldsymbol{C}\left(\boldsymbol{A}_{2n+1}-\boldsymbol{A}_{2n-1}\right)=\boldsymbol{M}_{\sigma}\boldsymbol{E}_{2n}\boldsymbol{R}_{2n}, \tag{1}$$

$$\boldsymbol{L}_{2n+1}=\boldsymbol{A}_{2n+1}{}^{\mathrm{T}}\boldsymbol{C}^{\mathrm{T}}\boldsymbol{M}_{\nu}\boldsymbol{C}\boldsymbol{A}_{2n+1}, \tag{2}$$

$$\tilde{\boldsymbol{E}}_{2n+2}-\boldsymbol{E}_{2n}=-\boldsymbol{A}_{2n+1}\boldsymbol{L}_{2n+1}{}^{-1}, \tag{3}$$

$$\boldsymbol{G}^{\mathrm{T}}\boldsymbol{M}_{\sigma}\boldsymbol{G}\boldsymbol{\Psi}_{2n+2}=-\boldsymbol{G}^{\mathrm{T}}\boldsymbol{M}_{\sigma}\tilde{\boldsymbol{E}}_{2n+2}, \tag{4}$$

$$\boldsymbol{E}_{2n+2}=\tilde{\boldsymbol{E}}_{2n+2}+\boldsymbol{G}\boldsymbol{\Psi}_{2n+2}, \tag{5}$$

$$\boldsymbol{R}_{2n+2}{}^{-1}=\boldsymbol{E}_{2n+2}{}^{\mathrm{T}}\boldsymbol{M}_{\sigma}\boldsymbol{E}_{2n+2}, \tag{6}$$

by starting the above from $\boldsymbol{E}_0=\boldsymbol{0}$ and $\boldsymbol{A}_{-1}=\boldsymbol{0}$. Here, $\boldsymbol{G}$ is the discrete gradient operator, $\boldsymbol{C}$ is the discrete curl operator [11], n is the stage number, and $\boldsymbol{R}_{2n}$ and $\boldsymbol{L}_{2n+1}$ are M-by-M matrices, respectively. The (i,j)-th entries of $\boldsymbol{M}_{\nu}$ and $\boldsymbol{M}_{\sigma}$ are expressed as

$$M_{\nu\,ij}=\int_V \nu\,\boldsymbol{N}^{\mathrm{f}}{}_i\cdot\boldsymbol{N}^{\mathrm{f}}{}_j\,\mathrm{d}V,\ M_{\sigma\,ij}=\int_V \sigma\,\boldsymbol{N}^{\mathrm{e}}{}_i\cdot\boldsymbol{N}^{\mathrm{e}}{}_j\,\mathrm{d}V \quad , \tag{7}$$

where ν is the magnetic reluctivity, σ is the conductivity, and $\boldsymbol{N}^{\mathrm{f}}_i$ and $\boldsymbol{N}^{\mathrm{e}}_i$ are the face-element and edge-element basis functions, respectively. Matrices $\boldsymbol{E}_{2n}$, $\boldsymbol{A}_{2n+1}$, and $\boldsymbol{\Psi}_{2n}$ are

$$\boldsymbol{E}_{2n}=\left(\boldsymbol{e}_{1,2n},\boldsymbol{e}_{2,2n},\cdots,\boldsymbol{e}_{M,2n}\right), \tag{8}$$

$$\boldsymbol{A}_{2n+1}=\left(\boldsymbol{a}_{1,2n+1},\boldsymbol{a}_{2,2n+1},\cdots,\boldsymbol{a}_{M,2n+1}\right), \tag{9}$$

$$\boldsymbol{\Psi}_{2n}=\left(\boldsymbol{\varphi}_{1,2n},\boldsymbol{\varphi}_{2,2n},\cdots,\boldsymbol{\varphi}_{M,2n}\right), \tag{10}$$

where $\boldsymbol{e}_{m,2n}$, $\boldsymbol{a}_{m,2n+1}$, and $\boldsymbol{\varphi}_{m,2n}$ are the basis vectors associated with the line integral of electric field, line integral of magnetic vector potential, and electric scalar potential, respectively. The first subscript indicates the corresponding port number, while the second subscript denotes the corresponding circuit element.

In the above procedure, (4) and (5) are novel additions to the existing CLN method for a cage IM described in [6] to ensure the condition of the sum of the bar currents always being zero by considering the circuit connection of the rotor bars. In the case where the number of rotor bars is divisible by the number of poles, only the odd SHs are included in the air-gap flux density waveform. Generally, however, the even SHs should also be considered in (8), (9), and (10) in the case where the number of the rotor bars is not divisible by the number of poles.

Here, we consider a cage IM with an axial length L_{a} and rotor radius R_{a}. Because the circumferential component of the air-gap

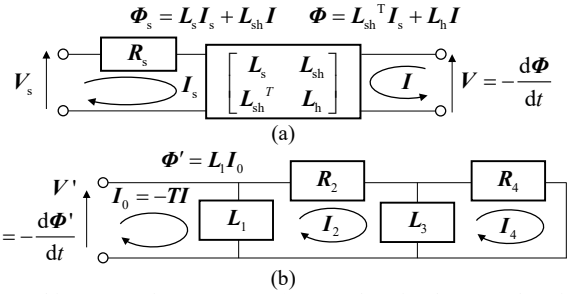

Fig. 1. Multiport CLN for cage IMs. (a) Stator domain. (b) Rotor domain.

magnetic field H_θ, the axial component of the air-gap electric field E_z, the axial component of the air-gap magnetic vector potential A_z, and the radial component of the air-gap flux density B_r are periodic functions with respect to the mechanical angle θ, they can be represented as follows:

$$H_\theta(\theta,t)=\sum_m\left[H_{cm}(t)\cos(mP_{\mathrm{n}}\theta)+H_{sm}(t)\sin(mP_{\mathrm{n}}\theta)\right], \tag{11}$$

$$\begin{aligned}E_z(\theta,t)&=\sum_m\left[E_{cm}(t)\cos(mP_{\mathrm{n}}\theta)+E_{sm}(t)\sin(mP_{\mathrm{n}}\theta)\right]\\&=-\frac{\partial A_z(\theta,t)}{\partial t}=-\frac{\partial}{\partial t}\sum_m\left[A_{cm}(t)\cos(mP_{\mathrm{n}}\theta)+A_{sm}(t)\sin(mP_{\mathrm{n}}\theta)\right]\end{aligned}, \tag{12}$$

$$B_r(\theta,t)=\frac{1}{R_{\mathrm{a}}}\frac{\partial A_z}{\partial\theta}=\frac{P_{\mathrm{n}}}{R_{\mathrm{a}}}\sum_m m\left[A_{sm}(t)\cos(mP_{\mathrm{n}}\theta)-A_{cm}(t)\sin(mP_{\mathrm{n}}\theta)\right], \tag{13}$$

where the subscript m indicates the order of the coefficient, and P_{n} is the number of pole-pairs. By substituting (11), (12), and (13) into the pointing vector and Maxwell stress tensor, we can obtain the power flowing into the rotor domain p_2 and the instantaneous torque τ as follows:

$$p_2=L_{\mathrm{a}}\int_0^{2\pi}E_zH_\theta\,R_{\mathrm{a}}\,\mathrm{d}\theta=\pi R_{\mathrm{a}}L_{\mathrm{a}}\sum_m\left(E_{cm}H_{cm}+E_{sm}H_{sm}\right), \tag{14}$$

$$\tau=R_{\mathrm{a}}L_{\mathrm{a}}\int_0^{2\pi}B_rH_\theta\,R_{\mathrm{a}}\,\mathrm{d}\theta=P_{\mathrm{n}}\pi R_{\mathrm{a}}L_{\mathrm{a}}\sum_m m\left(A_{sm}H_{cm}-A_{cm}H_{sm}\right). \tag{15}$$

The vectors $\boldsymbol{I}_{\mathrm{s}}$ and $\boldsymbol{V}_{\mathrm{s}}$ shown in Fig. 1 are expressed as

$$\boldsymbol{I}_{\mathrm{S}}=\left(I_{\mathrm{u}},I_{\mathrm{v}},I_{\mathrm{w}}\right)^{\mathrm{T}},\ \boldsymbol{V}_{\mathrm{S}}=\left(V_{\mathrm{u}},V_{\mathrm{v}},V_{\mathrm{w}}\right)^{\mathrm{T}}, \tag{16}$$

where I_{u}, I_{v}, I_{w}, and V_{u}, V_{v}, V_{w} are the phase currents and voltages, respectively. $\boldsymbol{V}$, $\boldsymbol{I}$, and $\boldsymbol{\Phi}$ in Fig. 1 are the vectors comprising the SHs of H_θ, E_z, and A_z. They are defined as

$$\boldsymbol{I}=\left(H_{\mathrm{c}1},H_{\mathrm{s}1},H_{\mathrm{c}2},H_{\mathrm{s}2},\cdots,H_{\mathrm{c}M},H_{\mathrm{s}M}\right), \tag{17}$$

$$\boldsymbol{V}=\pi R_{\mathrm{a}}L_{\mathrm{a}}\left(E_{\mathrm{c}1},E_{\mathrm{s}1},E_{\mathrm{c}2},E_{\mathrm{s}2},\cdots,E_{\mathrm{c}M},E_{\mathrm{s}M}\right), \tag{18}$$

$$\boldsymbol{\Phi}=\pi R_{\mathrm{a}}L_{\mathrm{a}}\left(A_{\mathrm{c}1},A_{\mathrm{s}1},A_{\mathrm{c}2},A_{\mathrm{s}2},\cdots,A_{\mathrm{c}M},A_{\mathrm{s}M}\right). \tag{19}$$

In this case, p_2 in (14) and τ in (15) can be written as

$$p_2=\boldsymbol{V}^{\mathrm{T}}\boldsymbol{I},\tau=\boldsymbol{B}^{\mathrm{T}}\boldsymbol{I},\boldsymbol{B}=P_{\mathrm{n}}\pi R_{\mathrm{a}}L_{\mathrm{a}}\left(A_{\mathrm{s}1},-A_{\mathrm{c}1},\cdots,MA_{\mathrm{s}M},-MA_{\mathrm{c}M}\right). \tag{20}$$

The torque and instantaneous secondary copper loss, including their ripples, can be evaluated based on the solutions of the CLN.

The Cauer circuits shown in Fig. 1 are connected based on the boundary conditions for the air-gap flux densities. When solving the circuit equations, the loop current is adopted for the unknown variables. Here, vector $\boldsymbol{I}_0$ comprises the loop currents at the first stage in the rotor domain, and $\boldsymbol{\Phi}'=\boldsymbol{L}_1\boldsymbol{I}_0$. The physical quantities in the respective domains are connected by $\boldsymbol{I}_0=-\boldsymbol{T}\boldsymbol{I}$ and $\boldsymbol{\Phi}'=\boldsymbol{T}\boldsymbol{\Phi}$ [6], where the transformation matrix $\boldsymbol{T}$ is given by

$$\boldsymbol{T}=\mathrm{blockdiag}[\boldsymbol{T}_1,\boldsymbol{T}_2,...,\boldsymbol{T}_M],\ \boldsymbol{T}_m=\begin{bmatrix}\cos mP_{\mathrm{n}}\omega t & -\sin mP_{\mathrm{n}}\omega t\\ \sin mP_{\mathrm{n}}\omega t & \cos mP_{\mathrm{n}}\omega t\end{bmatrix}, \tag{21}$$

where ω is the mechanical angular frequency.

To ensure stable calculation, the backward Euler method is adopted as a time integration scheme in the solution of the circuit equations corresponding to Fig. 1. When the number of stages N=2, the linear system of the circuit equations, where $\boldsymbol{I}_s$, $\boldsymbol{I}$, $\boldsymbol{I}_2$, and $\boldsymbol{I}_4$ are unknown variables, is given by

$$\begin{cases} \boldsymbol{R}_s\boldsymbol{I}_s + \boldsymbol{L}_s\dfrac{\mathrm{d}\boldsymbol{I}_s}{\mathrm{d}t} + \boldsymbol{M}_{sh}\dfrac{\mathrm{d}\boldsymbol{I}}{\mathrm{d}t} = \boldsymbol{V}_s, \quad (\boldsymbol{M}_{sh}^{\mathrm{T}}\boldsymbol{I}_s + \boldsymbol{L}_h\boldsymbol{I}) + \boldsymbol{T}^{-1}\boldsymbol{L}_1(\boldsymbol{T}\boldsymbol{I} + \boldsymbol{I}_2) = 0, \\ \boldsymbol{L}_1\dfrac{\mathrm{d}}{\mathrm{d}t}(\boldsymbol{I}_2 + \boldsymbol{T}\boldsymbol{I}) + \boldsymbol{R}_2\boldsymbol{I}_2 + \boldsymbol{L}_3\dfrac{\mathrm{d}}{\mathrm{d}t}(\boldsymbol{I}_2 - \boldsymbol{I}_4) = 0, \quad \boldsymbol{L}_3\dfrac{\mathrm{d}}{\mathrm{d}t}(\boldsymbol{I}_4 - \boldsymbol{I}_2) + \boldsymbol{R}_4\boldsymbol{I}_4 = 0 \end{cases} . \tag{22}$$

Because the coefficient matrix arising from (22) is symmetric, the conjugate gradient method with the localized incomplete Cholesky preconditioning [12] is adopted as an iterative solver.

B. Selection of SHs for Multiport CLN Method

The remaining task in the construction of the multiport CLN for cage IMs is to select the dominant components of the SHs. Because the increase in the number of SHs leads to large computational cost, it is desirable to apply as few components as possible to the multiport CLN method. All SHs included in the air-gap flux density waveform are directly extracted at an arbitrary slip using the time and space harmonic analysis proposed in [8]. The important operating point for cage IMs is the rated condition and maximum efficiency condition. In this case, however, owing to the small slip, large computational cost is required to obtain the air-gap flux density during a period corresponding to the slip frequency, although it can be reduced by using a polyphase time-periodic condition [8]. This method is called "Method A-m." When the slip s=1, the secondary current is maximum, and the effect of the rotor magnetomotive force is significant. This method is called "Method A-1." In the case of s=0, the air-gap flux density is evaluated near the rated condition. This method is called "Method A-0." Notably, in Method A-1 and Method A-0, the computational cost required to obtain the air-gap flux densities during a period is typically much smaller compared with Method A-m because there is no need to consider the slip frequency in the rotor region. In addition, Method A-0 is suitable for the nonlinear MOR based on the CLN method because the condition of s=0, which is close to the rated condition, enables us to evaluate the dominant SHs at a practical saturation level of the stator and rotor cores. In Methods A-m, A-1, and A-0, the SHs greater than 1% of the fundamental were selected as the dominant components.

Both p_2 in (14) and τ in (15) can be calculated from E_z in (12), H_θ in (11), and B_r in (13). Additionally, E_z is the time derivative of A_z as indicated in (12), and B_r is represented by a Fourier series expansion with A_{sm} and A_{cm}. Therefore, in theory, we should focus on H_θ and B_r simultaneously when extracting the dominant SHs, which are equivalent to $\boldsymbol{I}$ in (17) and $\boldsymbol{\Phi}$ in (19). The treatment of H_θ and B_r is discussed in detail in III-B.

The SHs in the air-gap flux density waveform comprise the fundamental, the stator and rotor slot harmonics, and their cross-interactions. The space order of these values can be estimated beforehand based on the number of stator slots n_s and number of rotor slots n_r. Generally, the order of potential stator slot harmonics is $in_s\pm1$, that of the rotor slot harmonics is $jn_r\pm1$, and that of the cross-interaction harmonics is $jn_r\pm in_s\pm1$, where i and j are integers. If all stator and rotor slot harmonics and their cross-interactions are considered, the number of potential SHs will be enormous and large computational cost will be required. Hence, only the stator and rotor slot harmonics were considered. This method is called "Method B."

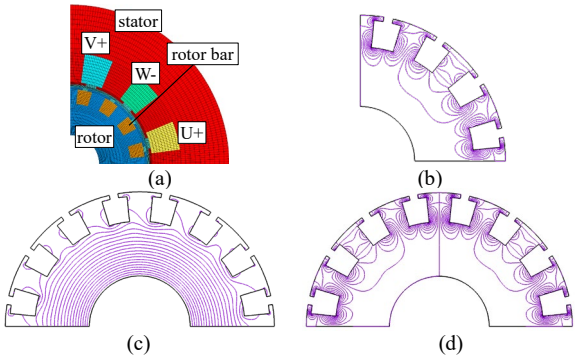

Fig. 2. Flux lines obtained by existing and developed CLN methods. (a) Mesh of one-pole model. (b) Reference. (c) Existing method. (d) Developed method.

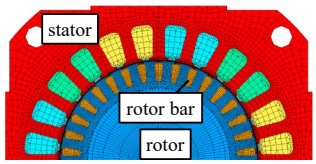

Fig. 3. Mesh of a practical cage induction motor.

III. Numerical Results

A. Verification of Developed Multiport CLN Method

To verify the developed CLN procedure in (1)–(6), the cage IM shown in Fig. 2(a) was investigated, in which the number of rotor bars per pole-pair is 8 and P_n=2. Fig. 2(b) shows the flux lines corresponding to the 17th SH at n=2, which were obtained from the one-pole model. Because the sum of the bar currents is strictly zero owing to the symmetry in the one-pole model, the numerical result shown in Fig. 2(b) is considered as the reference solution. Fig. 2(c) shows the flux lines calculated by the existing CLN method in the two-pole model. Owing to the numerical errors, the sum of the bar currents is not zero, and unphysical flux lines are obtained. The developed CLN procedure can obtain reasonable flux lines as shown in Fig. 2(d).

B. Extraction of Dominant SHs in Air-gap Flux Density

Fig. 3 shows the practical cage IM model, in which the number of rotor bars per pole-pair is 17 and P_n=2. The maximum efficiency of this IM is achieved at s=0.133. To reduce the computational cost required in Method A-m owing to the small slip, the polyphase time-periodic condition is used [8] by setting s=9/(4×17)≈0.132. The number of time steps per period was set to 360. In the case of the FEM, we determined an initial value to start a transient calculation based on the time-harmonic eddy-current analysis [13], where the slip frequency is applied to the rotor region. In contrast, the initial value for the CLN method was set to 0.

Fig. 4 shows the amplitude of the time and space harmonics of the radial and circumferential component B_r and B_θ, respectively, which were obtained using Methods A-m, A-1,

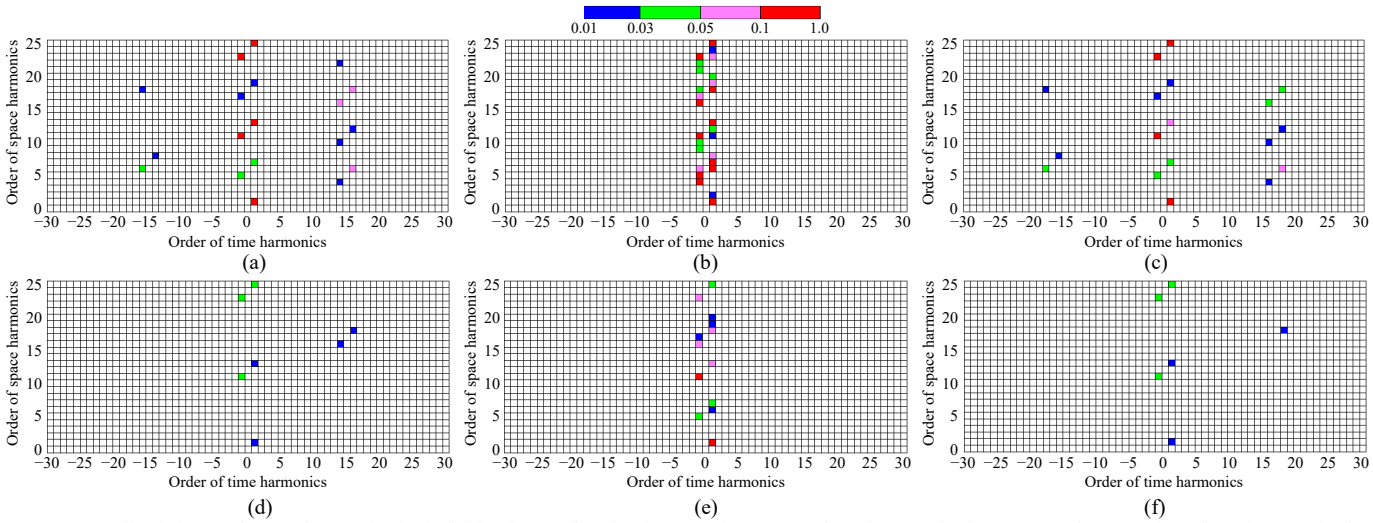

Fig. 4. Normalized time and space harmonics included in air-gap flux density waveform. (a) B_r based on Method A-m at s=9/(4×17). (b) B_r based on Method A-1. (c) B_r based on Method A-0. (d) B_θ based on Method A-m at s=9/(4×17). (e) B_θ based on Method A-1. (f) B_θ based on Method A-0.

and A-0. In Fig. 4, each component is normalized by the fundamental of B_r at each slip, which is the maximum component included in the air-gap flux density waveform; the components smaller than 1% of the fundamental are not shown. Although the fractional time harmonics occur at s=9/(4×17), they are rounded to the nearest integers in Fig. 4(a) and (d). This approximation for "time" order does not influence the appropriate selection of dominant "space" harmonics. The stator slot harmonics $6i\pm1$, the rotor slot harmonics $17j\pm1$, and their cross-interactions $17j\pm6i\pm1$ are included in Fig. 4 as main components. Because B_r is larger than B_θ and the significant time and space orders of B_θ are always consistent with those of B_r, as shown in Fig. 4, the dominant SHs are determined based on the time and space harmonic analysis of B_r.

Table I lists the number of selected SHs over 1% of the fundamental obtained by each method. Method A-1 extracts many SHs compared with the other methods. Because the primary current is maximum at s=1, a large voltage drop occurs at the primary impedance and the electromotive force decreases, which results in the decrease of the fundamental component of B_r. Thus, the amplitude of the higher-order SHs is relatively large and many SHs are selected by Method A-1. As s decreases, the primary current decreases, and the fundamental of B_r increases, which leads to a decrease in the number of selected SHs. The third column in Table I lists the calculation times to extract dominant SHs using the FEM. The values in parentheses denote the number of periods to obtain the air-gap flux density waveform in the steady state during a period corresponding to a slip frequency. Method A-m requires a 5-period transient analysis using the polyphase time-periodic condition.

In Fig. 5, the time variation of the phase current, torque, and secondary copper loss are compared at s=0.0588. In the CLN method, N was set to 3. The numerical results obtained by the FEM almost overlap with those obtained by the CLN based on Methods A-m, A-1, and A-0. In contrast, the torque and eddy-current loss waveforms obtained from the CLN based on Method B are different from the other results, because the cross-interaction components between the stator and rotor slots are ignored. The most accurate results are obtained by Method A-1

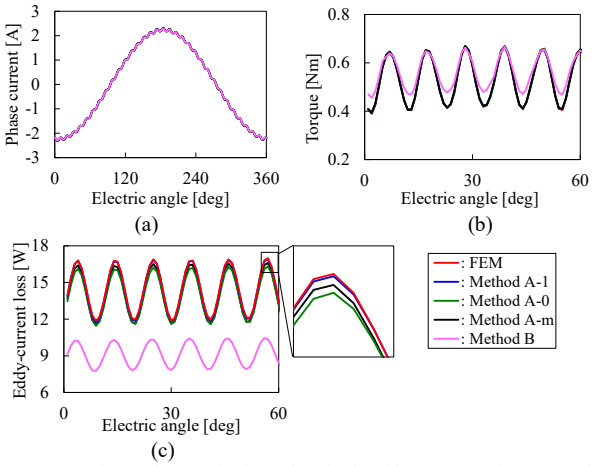

Fig. 5. Comparison of numerical results obtained by FEM and CLN methods at s=1/17. (a) Phase current. (b) Torque. (c) Secondary copper loss.

TABLE I
NUMBER OF SHS AND COMPUTATIONAL TIMES

Method	Number of SHs	Computational time [s]		
		Extracting dominant SHs	Deriving circuit parameters	Transient analysis
A-m	39	891.4 (5)	261.8	12.7 (10)
A-1	65	358.0 (2)	379.6	40.6 (10)
A-0	36	359.0 (2)	176.0	10.6 (10)
B	73	-	672.3	51.1 (10)
FEM	-	-	-	718.4 (4)

Intel Xeon Gold 6148 was used.

because the number of appropriately selected SHs is large. The fourth and fifth columns in Table I present the computational times to derive the circuit parameters using the FEM and the transient analysis at s=0.0588. The values in parentheses indicate the number of periods to obtain the steady-state solutions for a period. Because the initial value of the FEM is appropriately determined by the time-harmonic analysis, the number of periods to reach the steady state is smaller compared with the CLN methods. Although the CLN methods require computational time to extract the dominant SHs and derive the circuit parameters by the FEM, these calculations are carried out only once. Furthermore, a transient analysis by the CLN is much faster than the FEM. Therefore, the CLN method is

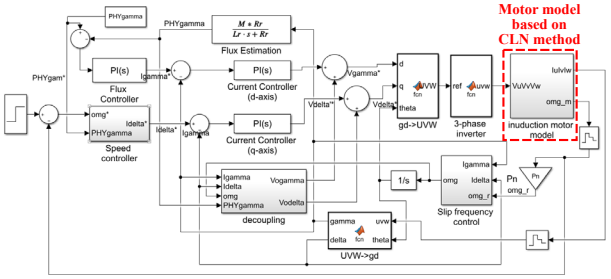

Fig. 6. Block diagram for circuit simulation coupled with control system.

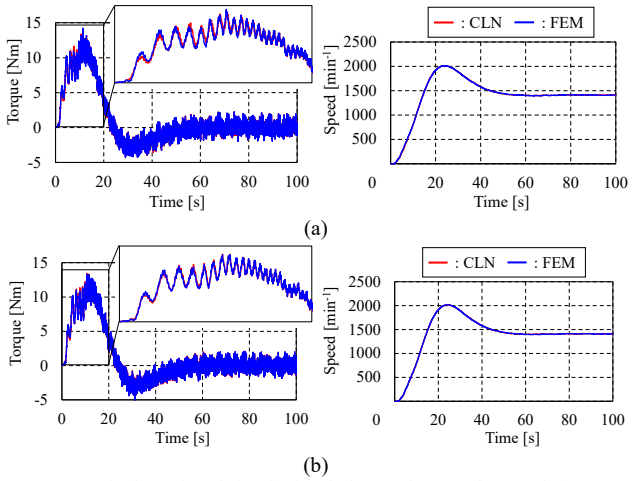

Fig. 7. Numerical results of circuit simulation under speed control. (a) Torque and speed using Method A-0. (b) Torque and speed using Method A-1.

suitable for situations where transient analyses are repeatedly carried out, for instance, in the design of electric motor control systems. From the viewpoint of computational accuracy and time, the use of either Method A-1 or Method A-0 is effective.

C. *Circuit Simulation Coupled with Control System*

The circuit simulation coupled with control system was conducted using the CLN as an accurate cage IM model. Fig. 6 shows the block diagram for the circuit simulation under speed control, which was implemented in Simulink; the CLN is represented by an S-Function block. The motion equation is coupled to consider the rotation of the rotor. The time step size was 20 μs and the starting transient for 100 ms was analyzed. The sine-triangle pulse width modulation was adopted for the inverter, and the carrier frequency was 5 kHz. The computations were carried out on Intel Core i7-8665U.

Fig. 7 show the time variations of the torque and speed when the dominant SHs were extracted using Method A-0 and Method A-1, respectively. The finite-element analysis of the IM coupled with the motion equation was also carried out by applying the line voltage obtained by the circuit simulation. The numerical results obtained by the FEM are shown in Fig. 7 as the reference solutions. The torque waveforms obtained by the FEM and CLN are slightly different just after starting the IM in Fig. 7(a). However, the effect of the slot and carrier harmonics on the torque is appropriately evaluated, and the numerical results obtained by the CLN are sufficiently accurate for its practical use. In Fig. 7(b), the CLN based on Method A-1 achieves the highly accurate circuit simulation, because the number of selected SHs is larger compared with Method A-0. The calculation times of the CLN with Method A-0 and Method A-1 are 30 s and 90 s, respectively. The FEM requires 35 min. Therefore, the effectiveness of the proposed CLN method in terms of computational accuracy and efficiency was confirmed.

IV. Conclusion

This study developed a novel CLN procedure for a cage IM to satisfy the condition of the sum of bar currents always being zero. Furthermore, a method is proposed to select the appropriate SHs based on time and space harmonic analysis. The developed motor model was applied to the circuit simulation of a cage IM under speed control. The results reveal that the proposed method can achieve high accuracy in circuit simulation with acceptable computational cost. In future work, we will combine the method for selecting appropriate SHs with the nonlinear MOR based on the CLN method and investigate a method for modeling skewed rotor slots.

Acknowledgment

This study was supported by JSPS KAKENHI (Grant-in-Aid for Scientific Research (C)) Grant Number JP20K04443.

References

[1] T. Henneron and S. Clénet, “Model order reduction applied to the numerical study of electrical motor based on POD method taking into account rotation movement,” *Int. J. Numer. Model.*, vol. 27, pp. 485-494, 2014.

[2] T. Shimotani, Y. Sato, T. Sato, and H. Igarashi, “Fast finite-element analysis of motors using block model order reduction,” *IEEE Trans. Magn.*, vol. 52, no. 3, Art. no. 7207004, 2016.

[3] A. Kameari, H. Ebrahimi, K. Sugahara, Y. Shindo, and T. Matsuo, “Cauer ladder network representation of eddy-current fields for model order reduction using finite element method,” *IEEE Trans. Magn.*, vol. 54, no. 3, Art. no. 7201804, 2018.

[4] T. Matsuo, A. Kameari, K. Sugahara, and Y. Shindo, “Matrix formulation of the Cauer ladder network method for efficient eddy-current analysis,” *IEEE Trans. Magn.*, vol. 54, no. 11, 7205805, 2018.

[5] N. Koester, O. Koenig, A. Thaler, and O. Bíró, “Application of model order reduction with Cauer ladder networks to industrial inductors,” *COMPEL*, https://doi.org/10.1108/COMPEL-02-2021-0058, 2021.

[6] T. Matsuo, K. Sugahara, A. Kameari, and Y. Shindo, “Model order reduction of an induction motor using a Cauer ladder network,” *IEEE Trans. Magn.*, vol. 56, no. 3, Art no. 7514704, 2020.

[7] H. Eskandari and T. Matsuo, “Cauer ladder network representation of a nonlinear eddy-current field using a first-order approximation,” in *IEEE Trans.Magn.*, vol. 56, no. 2, Art no. 7505904, 2020.

[8] H. Mikami, K. Ide, M. Takahashi, and K. Kajiwara, “Dynamic harmonic field analysis of an inverter-fed induction motor for estimating harmonic secondary current and electromagnetic force,” *IEEE Trans. Energy Convers.*, vol. 14, no. 3, pp. 464–470, 1999.

[9] H. Ebrahimi, K. Sugahara, T. Matsuo, H. Kaimori, and A. Kameari, “Modal decomposition of 3-D quasi-static Maxwell equations by cauer ladder network representation”, *IEEE Trans. Magn.*, vol. 56, no. 3, Art. no. 7513004, 2020.

[10] M. Tobita and T. Matsuo, “Nonlinear Model Order Reduction of Induction Motors Using Parameterized CLN Method”, *Proc. of 23rd Conference on the Computation of Electromagnetic Fields*, OB1-1, 2022.

[11] A. Bossavit, “Computational Electromagnetism,” New York: Academic, 1998.

[12] T. Iwashita and M. Shimasaki, “Parallel processing of 3-D eddy current analysis with moving conductor using parallelized ICCG solver with renumbering process,” *IEEE Trans. Magn.*, vol. 36, no. 4, pp. 1504–1509, 2000.

[13] K. Yamazaki, “An efficient procedure to calculate equivalent circuit parameter of induction motor using 3-D nonlinear time-stepping finite-element method,” *IEEE Trans. Magn.*, vol. 38, no. 2, pp. 1281-1284, 2002.